# Importance of Capturing Non-linear Viscoelastic Material Behavior in Tire Rolling Simulations

Biswanath Nandi*
Biswanath.Nandi@3ds.com
Dassault Systemes SIMULIA Corp.
166 Valley Street
Providence, RI-02903
USA

Tod Dalrymple
Tod.Dalrymple@3ds.com
Dassault Systemes SIMULIA Corp.
166 Valley Street
Providence, RI-02903
USA

Jiang Yao
Jiang.Yao@3ds.com
Dassault Systemes SIMULIA Corp.
166 Valley Street
Providence, RI-02903
USA

Ireneusz Lapczyk
Eric.Lapczyk@3ds.com
Dassault Systemes SIMULIA Corp.
166 Valley Street
Providence, RI-02903
USA

Presented at the
8-10 September 2014
Meeting of the Tire Society

*Presenter /Corresponding Author

**Abstract:** Tire engineers are always interested in predicting rolling resistance using a finite element analysis tool. Rolling resistance mainly depends on the viscoelastic energy dissipation of the rubber material used in the tires. Computation of viscoelastic energy dissipation with linear viscoelasticity approach for finite strains is inaccurate and remains a technical challenge so far. With the recent implementation of the Parallel Rheological Framework model (PRF) in Abaqus[1,2], a non-linear viscoelastic approach, the viscoelastic energy dissipation is computed more accurately than it was possible before. This paper provides a theoretical background of the linear and non-linear viscoelastic models available in Abaqus. It also describes a methodology to calibrate the parameters of the PRF model starting from material test data.
In addition to the material calibration procedure, this paper also briefly describes a simulation methodology to predict temperature distribution in a rolling tire due to viscoelastic energy dissipation in the rubber material.

**Keywords:** Linear viscoelasticity, nonlinear viscoelasticity, rolling resistance, viscous energy dissipation, finite-strain viscoelasticity, Parallel Rheological Framework.

## 1.0 Introduction:

Rubber material has found wide usage in tires because of its properties of elasticity and resilience. However, unlike metals which require few parameters to characterize the material behavior, the material behavior of rubber is very complex. The mechanical behavior of rubbers is highly nonlinear and further complicated by its sensitivity to temperature, environment, strain history, loading rate, amount of strain, ingredients etc. In last several decades, a significant progress has been made in characterizing the hyperelastic part of a rubber material. There are many numerical models available to characterize the hyperelastic behavior; however, there has been little progress made in describing the viscoelastic behavior of rubber materials. So far, only the linear viscoelastic material models are implemented in the numerical tools to characterize the viscoelastic part with limited accuracy.

In modern-day rubbers, filler materials such as carbon-black and silica are widely used, and these filled rubber materials[3,4] exhibit highly nonlinear rate dependent[5,6] behavior which cannot be described by the traditional linear viscoelasticity models. Examples of such behaviors include the amplitude dependency of the dynamic stiffness, also known as Payne or Fletcher-Gent effect[7], and preload dependent relaxation behavior, to name a few. These materials also exhibit stress softening[8] behavior (or Mullins effect) after a virgin specimen is subjected to an initial load, and an associated permanent set upon removal of the load.

In 2012, a non-linear viscoelasticity material model was implemented in the commercial finite element analysis software Abaqus (Abaqus 6.12 Documentation). The material model is known as Parallel Rheological Framework model (PRF). The framework is based on the superposition of finite-strain viscoelastic and elastoplastic networks in parallel, so that the overall stress response is additive. For each network the model assumes a multiplicative split of the deformation gradient into an elastic component and a viscous or plastic component, depending on whether the network is viscoelastic or elastoplastic, respectively. The PRF model is described in details in the next few chapters, and a calibration method of the PRF model parameters is also discussed.

**2.0 Linear and Nonlinear Viscoelasticity:** All materials behave non-linearly in some fashion. But often material behavior can be approximated as linear, such as steel at strain levels below its yield point. As shown in the FIG. 2, steel behaves as a purely elastic material below its yield point, loading and unloading occurs on the same path. Elastomers have a highly random molecular chain structure as shown in FIG. 1. As the material experiences strain, these chains realign to carry the load. This realignment results in a non-linear material response that varies with strain level and time. To capture the non-linearity as functions of strain and time, the material model needs to capture both an hyperelastic as well as a viscoelastic component (FIG. 3). Viscous materials lose energy when a load is applied and subsequently removed. Energy dissipation through hysteresis is represented by the area between the loading and unloading curves in a load-deformation cycle. At high elongations, the hysteresis is much greater; this is associated with crystallization. Rapidly repeated cyclic loading will results in heat generation within the material..

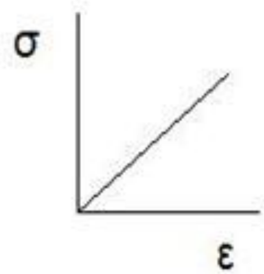


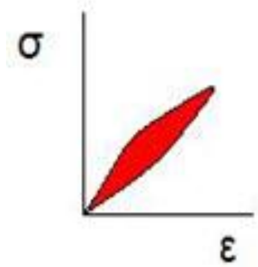


FIG. 1: Molecular Rearrangements FIG. 2 Elastic Behavior FIG. 3 Viscoelastic Behavior

## *2.1 Stress Relaxation Test:*

A stress relaxation test measures the stress (force) response as a function of time while strain (displacement) is held constant on the specimen as shown in the FIG. 4.

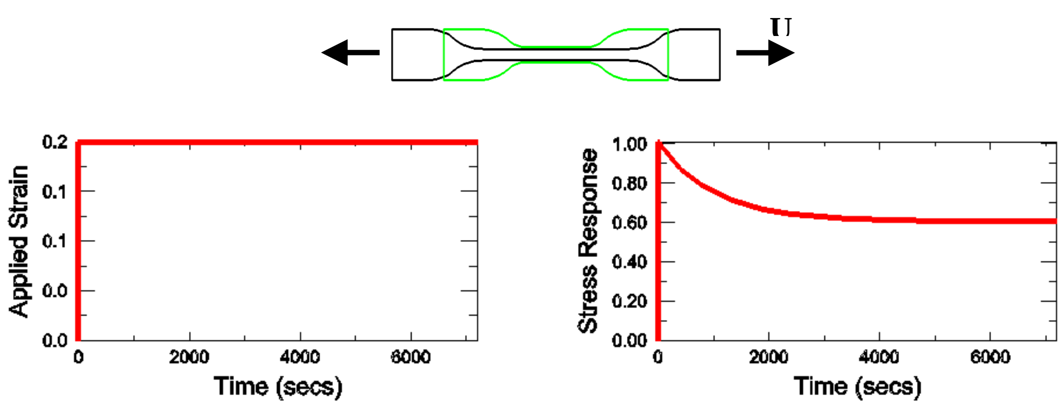


FIG. 4: Stress Relaxation Test

## *2.2 Creep Test:*

A creep test measures strain (displacement) response as function of time while stress (force) is held constant on the specimen as shown in the FIG. 5. For a prescribed stress (force), viscoelastic materials creep over time.

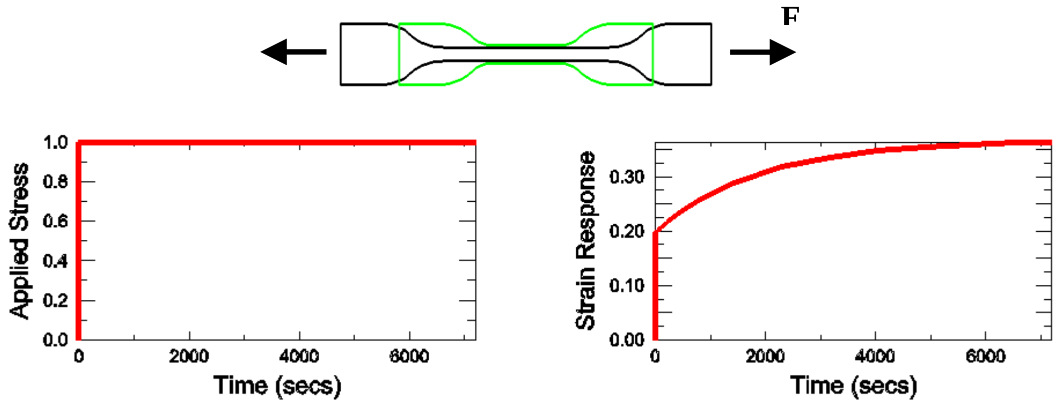


FIG. 5: Creep Test

*2.3 How to Determine the Non-Linearity?* Linear viscoelasticity means that the time dependent shear modulus of the material is not a function of stress magnitude. In other words, it means that the relaxation rates are independent of the strain or stress imposed. From a practical perspective, one tests the validity of “linear” viscoelasticity by testing at multiple load levels and overlaying the normalized stress relaxation plots. FIG. 6 shows the stress relaxation test data for a silicone rubber at 30% and 50% strain levels. FIG. 7 shows the normalized stress relaxation plots overlaid to each other indicating that the material behavior can be assumed as linear viscoelastic.

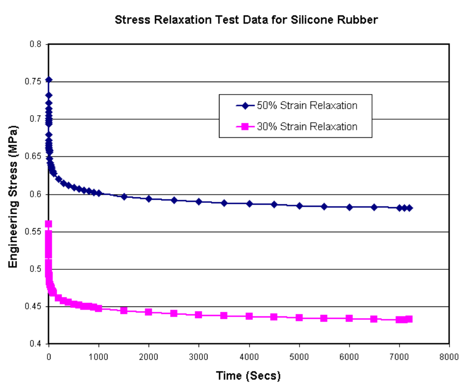


FIG. 6: Stress Relaxation Test data

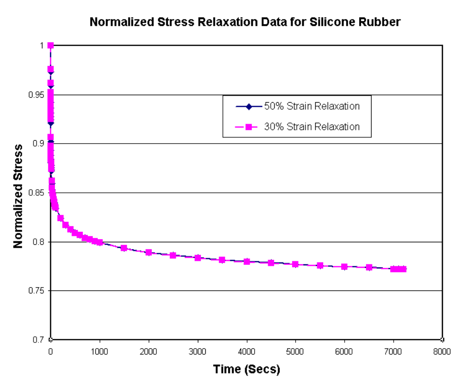


FIG. 7: Normalized Stress Relaxation Plots

FIG. 8 shows stress relaxation test data at different strain levels and the normalized stress relaxation plots of an elastomer, and these plots indicate that the viscoelastic behavior is nonlinear. For describing this kind material behavior, the PRF material model will be the appropriate choice.

Courtesy of Axel Products Inc.

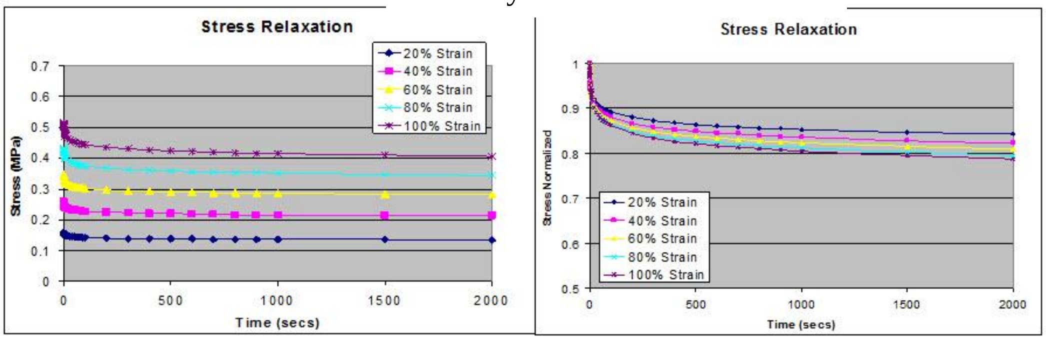


FIG. 8: Stress Relaxation Test Data

## 2.3 *Linear Viscoelasticity Theory*

The finite-strain viscoelasticity theory implemented in Abaqus is a time domain generalization of either the hyperelastic or hyperfoam constitutive models. It is assumed that the instantaneous response of the material follows from the hyperelastic constitutive equations

$$\tau_0(t) = \tau_0^D(\bar{\mathbf{F}}(t) + \tau_0^H(t) \qquad (1)$$

for an incompressible material. In the above, $\tau_0^D$ and $\tau_0^H$ are, respectively, the deviatoric and the hydrostatic parts of the instantaneous Kirchhoff stress $\tau_0$ . $\bar{\mathbf{F}}$ is the "distortion gradient" related to the deformation gradient **F** by

$$\bar{\boldsymbol{F}} = \frac{\boldsymbol{F}}{J^{1/3}} \qquad (2)$$

where
$J = \det(\mathbf{F})$ is the volume change.

Using integration by parts and a variable transformation, the basic hereditary integral formulation for linear isotropic viscoelasticity can be written in the form

$$\sigma(t) = 2G_0 e(t) + \int_0 2G(\tau')e(t-t')d\tau' + I\left(K_0 \emptyset(t) + \int_0 K(\tau')\emptyset(t-t')d\tau'\right) \quad (3)$$

or entirely in terms of stress quantities,

$$\sigma(t) = S_0(t) + \int_0^\tau \frac{\dot{G}(t')}{G_0} S_0(t-t')d\tau' + I\left(p_0(t) + \int_0^\tau \frac{\dot{K}(\tau')}{K_0} p(t-t')d\tau'\right) \qquad (4)$$

where $\tau$ is the reduced time, $\dot{G}(t') = dG(\tau')/d\tau'$ , and $\dot{K}(t') = dK(\tau')/d\tau'$ . $G_0$ and $K_0$ are the instantaneous small-strain shear and bulk moduli, and G(t) and K(t) are the time-dependent small-strain shear and bulk relaxation moduli. Recall that the reduced time represents a shift in time with temperature and is related to the actual time through the differential equation

$$d\tau' = \frac{dt'}{A_\theta(\theta(t')} \tag{5}$$

where $\theta$ is the temperature and $A_\theta$ is the shift function.

## 2.3 *Numerical Implementation of Linear Viscoelasticity*

Abaqus assumes that the viscoelastic material is defined by a Prony series expansion of the dimensionless relaxation modulus:

$$gR(t) = \sum_{i=1}^{N} \dot{g}_i^{\,P}(1 - e^{-t/\tau_i^G}) \tag{6}$$

where $N$, $\dot{g}_i^{\,P}$, and $\tau_i^G$, $i = 1, 2, \ldots, N$, are material constants. For linear isotropic elasticity, substitution in the small-strain expression for the shear stress yields

$$\tau(t) = G_0(\gamma - \sum_{i=1}^{N} \gamma_i) \tag{7}$$

$$\textit{where} \quad \gamma_i = \frac{\dot{g}_i^{\,P}}{\tau_i^G} \int_0^t e^{-\frac{s}{\tau_i^G}} \gamma(t-s)ds \tag{8}$$

The $\gamma_i$ are interpreted as state variables that control the stress relaxation, and

$$\gamma^{cr} = \sum_{i=1}^{N} \gamma_i \tag{9}$$

is the “creep” strain: the difference between the total mechanical strain and the instantaneous elastic strain (the stress divided by the instantaneous elastic modulus).

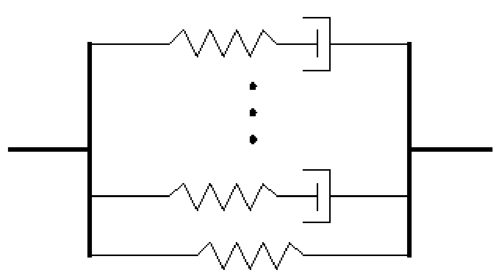

FIG. 9: Generalized Maxwell Model

Linear and finite-strain viscoelasticity are idealized as series pairs of springs and dashpots in parallel with a spring as shown in FIG. 9. The number of dashpots is equal to the number of terms in the Prony series representing the stress response (the number of terms needed to fit the test data for the time domain of interest). In the above implementation, creep strain is not computed separately for each network; hence, energy dissipation due to hysteresis with linear viscoelasticity approach is approximate. Please note that Abaqus/Explicit does not compute the energy dissipation with linear viscoelasticity, the quantities CENER (viscous energy dissipation per unit volume) and ALLCD (Creep dissipation energy for the whole model) are reported as zero.

## 3.0 PRF Model Overview

The framework consists of multiple elastic and viscoelastic networks connected in parallel, as shown in the FIG. 10. The number of viscoelastic networks, *N*, can be arbitrary; however, at most one purely elastic or equilibrium network (network 0 in FIG. 10) is allowed in the model. If the elastic network is not defined, the stress in the material will relax completely over time; otherwise, the stress will relax to a residual value, which is different from zero.

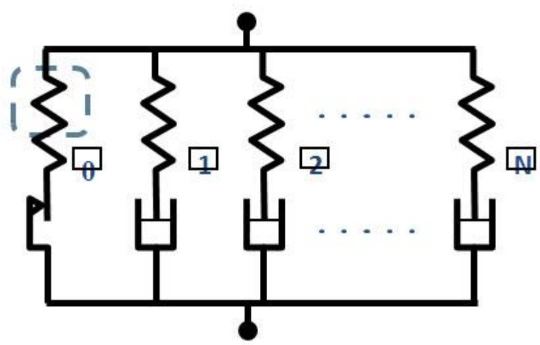


$$\sum_{i=0}^{N} s_i = 1$$

FIG. 10: Schematic Representation of the PRF Model

### *3.1 Elastic Response*

The elastic response in each network is assumed to be determined by a hyperelastic strain energy potenial in the

$$W = W_i\,(C_i^e) \qquad i = \ldots N \tag{10}$$

Where $C_i^e = (F_i^e)^T . F_i^e$ is the elastic right Cauchy-Green tensor in each network.
We further assume that all networks have the same functional form of the strain energy potential and that the total strain energy $W_t$ is equal to the weighted sum of the strain energies of all the networks.

$$W_T = \sum_{i=0}^{N} S_i \, W(C_i^e), \tag{11}$$

Where $S_i$ denotes the ith network's stiffness ratio, which represents the volume fraction of the network. The stiffness ratios are material parameters to be determined and must satisfy the relation.

$$\sum_{i=0}^{N} S_i = 1 \tag{12}$$

The total stress response can be derived from the strain energy potential as:

$$\tau = \sum_{i=0}^{N} S_i \left\{ F_i^e . 2 \frac{\partial W(C_i^e}{\partial C_i^e} . (F_i^e)^T \right\} = \sum_{i=0}^{N} S_i \, \tau_i \tag{13}$$

## *3.1 Viscous Behavior of Each Network*

In the previous section, the elastic part of the deformation gradient was specified. In this section, we specify the evolution for the inelastic part of the deformation gradient and provide the description of the constitutive response for a single viscoelastic network.

We assume the existence of the creep potential, which has the following general form

$$\mathrm{G}^{\mathrm{cr}} = \mathrm{G}^{\mathrm{cr}}(\sigma) \tag{14}$$

Where σ is the Cauchy stress. If the potential is specified, the flow rule can be obtained from

$$D^{cr} = \dot{\lambda} \frac{\partial G^{cr}(\sigma)}{\partial \sigma} \tag{15}$$

where $\mathrm{D}^{\mathrm{cr}}$ is the symmetric part of the velocity gradient, $L^{\mathrm{cr}}$ , expressed in the current configuration and $\dot{\lambda}$ is the proportionality factor. In this model the creep potential is given by

$$G^{cr} = \bar{q} \tag{16}$$

and the proportionality factor is taken as $\dot{\lambda} = \dot{\bar{\epsilon}}^{cr}$, where $\bar{q}$ is the equivalent deviatoric Cauchy stress and $\dot{\bar{\epsilon}}^{cr}$ is the equivalent creep stain rate. In this case the flow rule has the form

$$D^{cr} = \frac{3}{2q} \dot{\bar{\epsilon}}^{cr} \tag{17}$$

or, equivalently

$$D^{cr} = \frac{3}{2\tilde{q}} \dot{\bar{\epsilon}}^{cr} \; \bar{\tau} \tag{18}$$

Where $\tau = J\sigma$ is the Kirchhoff stress, J is the determinant of **F**, $\bar{\sigma}$ is the deviatoric Cauchy stress, $\bar{\tau}$ is the deviatoric Kirchhoff stress, and $\tilde{q} = J\bar{q}$ . To complete the derivation, the evolution law for $\dot{\bar{\epsilon}}^{cr}$ must be provided. In this model $\dot{\bar{\epsilon}}^{cr}$ can be determined from the following creep law models.

### *3.2 Power Law Strain Hardening Model*

The power-law strain hardening model is available in the form

$$\dot{\bar{\epsilon}}^{cr} = \left(A\, \tilde{q}^{n} \left[(m+1)\, \bar{\epsilon}^{cr}\right]^{m}\right)^{\frac{1}{m+1}} \tag{19}$$

where $\dot{\bar{\epsilon}}^{cr}$ is the equivalent creep strain rate, $\bar{\epsilon}^{cr}$ is the equivalent creep strain, $\tilde{q}$ is the equivalent deviatoric Kirchhoff stress, and *A*, *m*, and *n* are material parameters.

### *3.1 Power Law Model*

The power law model is available in the form

$$\dot{\bar{\epsilon}}^{cr} = \dot{\epsilon}_0 \left( \left(\frac{\tilde{q}}{q_0 + a\langle p\rangle}\right)^{n} \left[(m+1)\, \bar{\epsilon}^{cr}\right]^{m} \right)^{\frac{1}{m+1}} \tag{20}$$

Where $\dot{\bar{\epsilon}}^{cr}$ is the equivalent creep strain rate, $\bar{\epsilon}^{cr}$ is the equivalent creep strain, $\tilde{q}$ is the equivalent deviatoric Kirchhoff stress, p is the Kirchhoff pressure, and $q_0$ , *m*, *n*, *a* and $\dot{\epsilon}_0$ are material parameters.

### *3.3 Hyperbolic-Sine Law Model*

The hyperbolic-sine law is available in the form

$$\dot{\bar{\epsilon}}^{cr} = A\, (\sinh B\tilde{q}\,)^{n} \tag{21}$$

where $\dot{\bar{\epsilon}}^{cr}$ and $\tilde{q}$ are defined above, and *A*, *B*, and *n* are material parameters.

### *3.4 Bergstrom-Boyce Model*

The Bergstrom-Boyce model is available in the form

$$\dot{\bar{\epsilon}}^{cr} = A(\lambda^{cr} - 1 + E)^{C} (\tilde{q})^{m}\, , \tag{22}$$

where $\lambda^{cr} = \sqrt{\frac{1}{3}\, \mathrm{I} : \mathrm{C}^{cr}}$ and $\dot{\bar{\epsilon}}^{cr}$ and $\tilde{q}$ are defined above, and *A*, *m*, *C*, and *E* are material parameters.

## 4.0 Calibration of the PRF Model Parameters

As described in the section 2.3, the PRF model can be the best choice to describe a nonlinear viscoelastic material behavior. However, it is not a trivial task to compute the PRF material parameters from the test data. In this section, a calibration approach has been discussed to construct a PRF model from the stress relaxation test data.

## *4.1 Step 1: Calculate Hyperelastic Model Parameters*

Test data shown in FIG 8 was considered for this exercise. For constructing a short term hyperelastic model, the stress-strain data from each of these curves at 0.1 sec were taken as shown in FIG. 11. The parameters for a short term Yeoh hyperelastic model were calculated by inserting the above stress-strain data in Abaqus/CAE. The following parameters are computed and the correlation between the test and the Abaqus prediction is shown in FIG. 12.

Courtesy of Axel Products Inc.

| At time = 0.1 secs | |
|---|---|
| Eng. Strain | Eng. Stress |
| 0.00 | 0 |
| 0.10 | 0.0981 |
| 0.20 | 0.1593 |
| 0.30 | 0.2113 |
| 0.40 | 0.2575 |
| 0.50 | 0.3025 |
| 0.60 | 0.3466 |
| 0.70 | 0.3910 |
| 0.80 | 0.4329 |
| 0.90 | 0.4745 |
| 1.00 | 0.5147 |

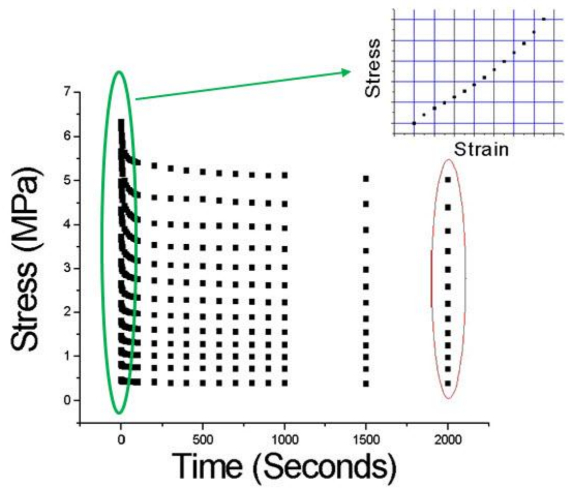


FIG. 11: Calibration of the Hyperelastic Model Parameters

## *4.1 Step 2: Calculate Linear Viscoelastic Model Parameters*

The next step is to calculate the Prony terms to describe the viscoelastic behavior. Even though, it was noted earlier from FIG. 8 that the material behavior cannot be described by a linear viscoelastic model, Prony model is considered for obtaining the starting values of the PRF model parameters. For calculating the Prony terms, the stress relaxation data at 30% strain were used. FIG. 13 shows the Prony series terms computed by Abaqus/CAE and the response of the model at different strains. Hyperelastic and Prony series model results match very well to the test data at 30% strain as the Prony terms were calculated based on the data at 30% strain. However, the results do not match as well at higher strains because of the nonlinear behavior.

```
*MATERIAL,
 NAME= Material-1
*HYPERELASTIC,YEOH,
 MODULI=INSTANT
.1524,-.00791,.0023,.123,0,0, 0
```

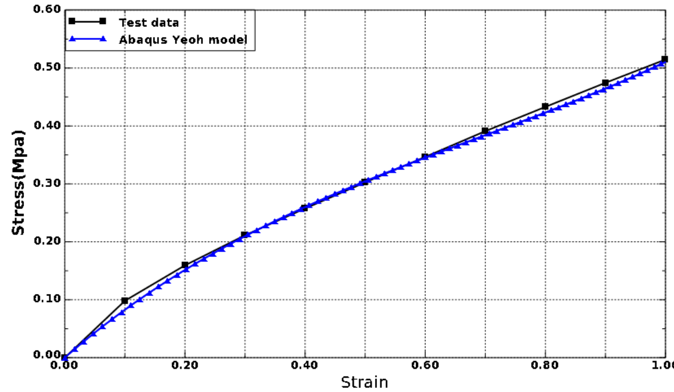


FIG. 12: Abaqus Yeoh Model Uniaxial Response

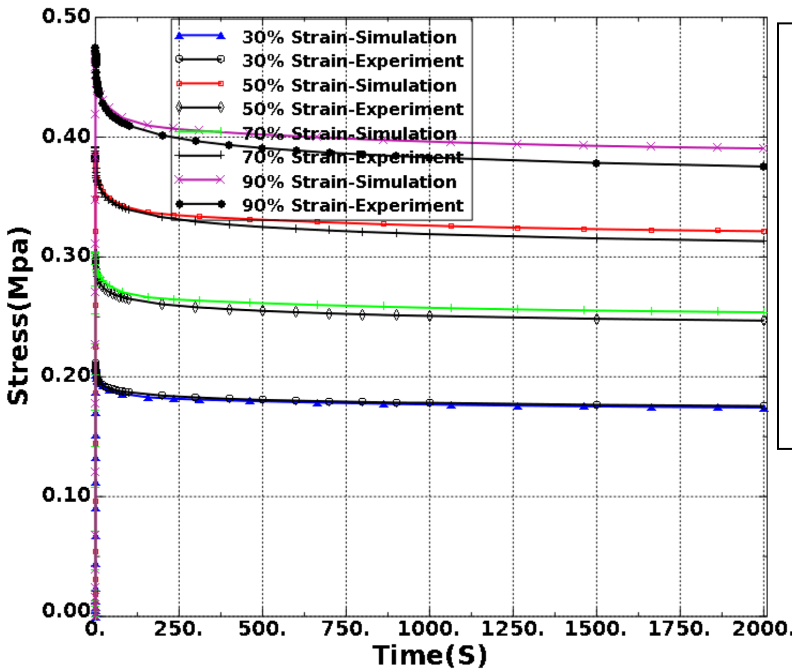


C10 = .1524
C20 = -.0079
C30 = .0023
D1 = 0.1230
g1 = .0560
tau1 = 1.354
g2 = .06761
tau2 = 49.5647
g3 = .0529
tau3 = 986.9

FIG. 13: Hyperelastic and Prony Response

## *4.1 Step 3: Convert the Prony Terms to Linearized PRF Parameters*

PRF power law strain hardening model is selected for describing the creep behavior of this material. Equation 17 describes the power law strain hardening model. Note that the model becomes linear when m=0 and n=1.0. To compute the starting values of the parameters of this model, the Prony terms are mapped to the linearized version of the PRF power law strain hardening model.

TABLE 1: Parameter Conversion

| Prony Series Parameters | | Power Law Strain Hardening Linearized Model Parameters | |
|---|---|---|---|
| | | SR_i=g_i<br>A_i=1/(6*g_i*tau_i*C10) | |
| C10 | 0.1523 | m | 0.0 |
| D1 | .1230 | n | 1.0 |
| g1 | 0.0561 | SR1 | 0.0561 |
| tau1 | 1.3547 | A1 | 14.4040 |
| g2 | 0.0676 | SR2 | .0676 |
| tau2 | 49.5650 | A2 | .3265 |
| g3 | 0.0530 | SR3 | 0.0676 |
| tau3 | 986.900 | A3 | .02093 |

Table 1 shows the relationship between the Prony terms and the power law strain hardening model parameters. FIG. 14 shows the results of the PRF model with the initial values of the parameters. Note that the Hyperelastic and Prony model results shown in FIG. 13 and the Hyperelastic and the linearized PRF model results shown in FIG. 14 are similar, and this is expected as the initial values of power law model parameter are computed from the Prony series coefficients.

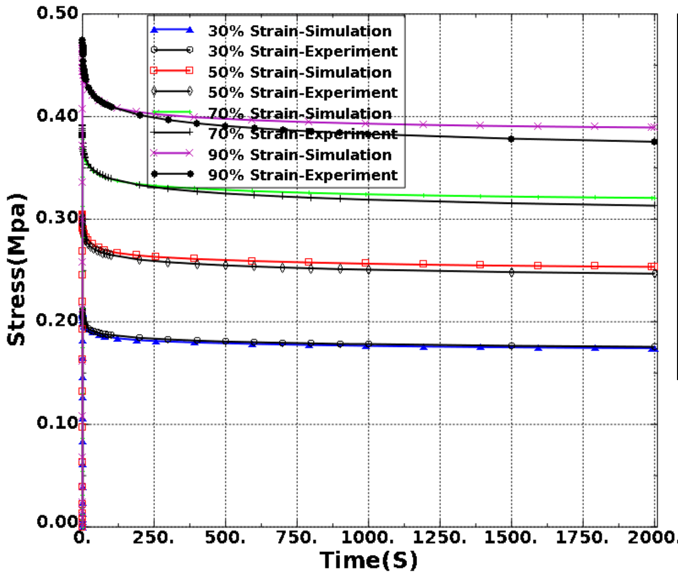


C10 = 0.1523
C20 = -.0079
C30 = 0.0023
D1 = 0.1230
SR1 = .0561
A1 = 14.4040
SR2 = .0676
A2 = .3265
SR3 = .05296
A3 = 0.0209

FIG. 14: Hyperelastic and Linearized PRF model Response

## *4.1 Step 4: Optimize the Parameters using Isight*

In this step, all the parameters of the hyperelastic and the PRF model are optimized using Isight 5.8 and Abaqus 6.13-1. A finite element model with four elements (unit cubes) is constructed for this purpose. Each of these elements is pulled with different displacements to achieve 30%, 50%, 70% and 90% strains. Reaction forces for each of these elements are recorded. As all the elements are unit cubes, the reaction forces (engineering stresses) are directly compared with the stress relaxation test data using the Isight Data Matching component.

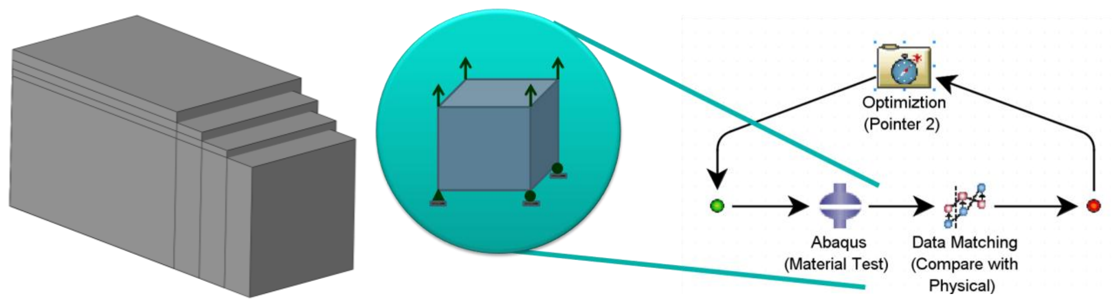


FIG. 15: PRF Model Parameters Calibration using Isight

FIG. 15 shows a Isight Sim-flow which includes an optimization technique on the Abaqus model to calibrate the PRF model parameters.

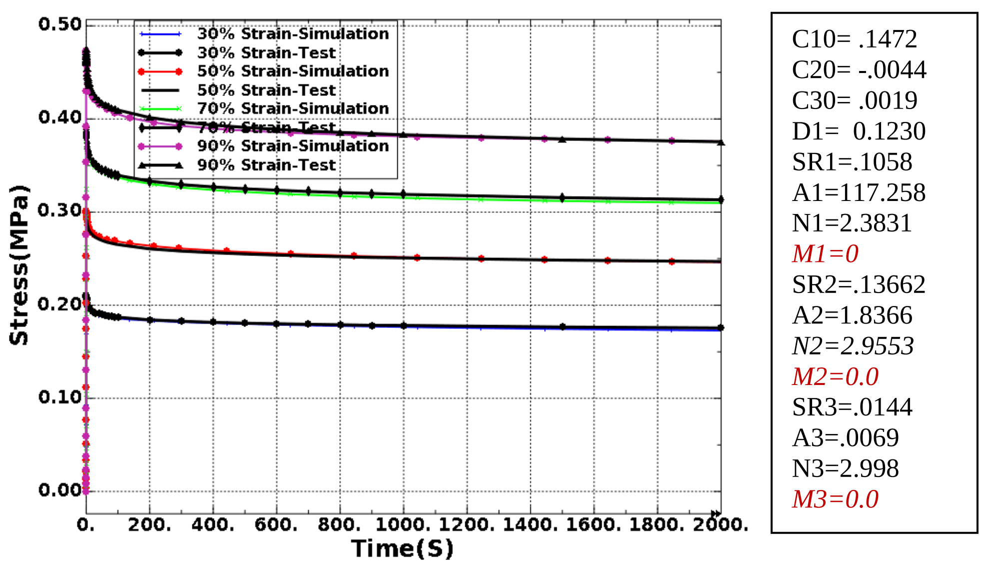


FIG. 16: PRF Model response with the optimized parameters (excluding m)

FIG. 16 shows the resulting parameters obtained from the optimization analysis and the PRF model response. In the first optimization run, the parameter ‘m’ was assumed to be zero and was excluded from the optimization. FIG. 16 shows that the PRF model with the optimized parameters is able to capture the behavior accurately at all strains. Values of the N parameter indicate the rate of relaxation. It is expected that N would be greater than 1 to capture the higher rate of relaxation at higher load levels. For this mildly nonlinearly viscous material the N parameters are in the range of 2~3.

In the second optimization run, the parameter ‘*m’* was also included. FIG. 17 shows the results of this run. Note that the values of ‘m’ are quite small. In the next optimization run, only two viscous networks were used. FIG. 18 shows the response of the PRF model with two networks. It is important to note that two viscous networks are enough to capture the nonlinear viscoelastic behavior of this particular elastomer. To save computational cost, a minimum number of viscous networks should be used to represent the nonlinear behavior as the computational cost increases with addition of each network.

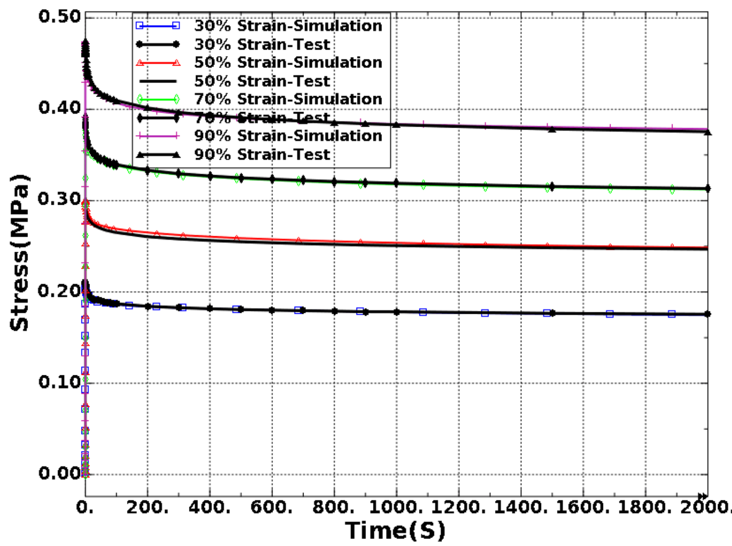


C10= .1474
C20= -.0044
C30= .0020
D1= 0.1230
SR1=.1047
A1=163.512
N1=2.436
*M1=-.00601*
SR2=.14173
A2=1.3927
*N2=2.7965*
*M2=-.0506*
SR3=.01649
A3=.0069
N3=1.9730
*M3=-9.9e-9*

FIG. 17: PRF Model Response with the Optimized Parameters (including m)

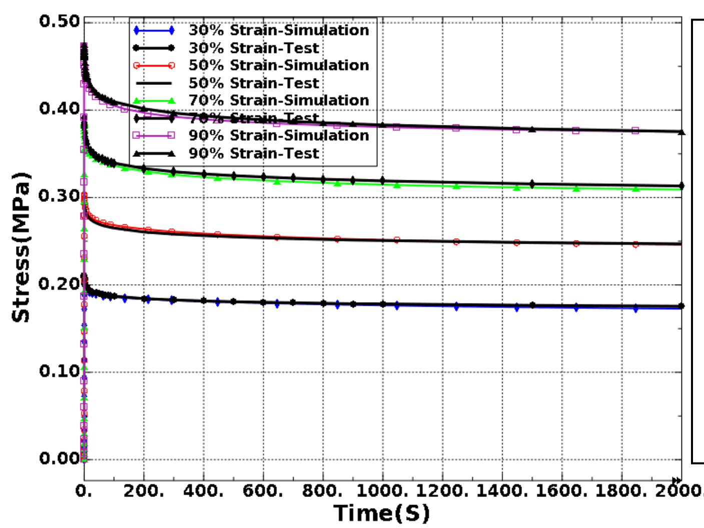


C10 = .1474
C20 = -.00447
C30 = .0020
D1 = 0.1230
SR1 = .1047
A1 = 63.512
N1 = 2.4361
*M1 = -.0060*
SR2 = .1417
A2 = 1.3927
*N2 = 2.7965*
*M2 = -.0506*

FIG. 18: PRF Model Response with two viscous networks

## 5.0 Tire Rolling Simulation

The steady state transport capability available in Abaqus/Standard provides an efficient solution method for the steady rolling on a flat road or on a drum, as is frequently performed experimentally. Unfortunately, the PRF model is not yet supported in the steady state transport technique; therefore, a simulation methodology for tire rolling simulations using Abaqus/Explicit is discussed in the following sections.

## *5.1 3D Tire Model Development*

Building a 3D tire model consists of several analyses run in sequence. FIG. 19 visually describes the steps involved in a typical tire rolling simulation. Tires are axisymmetric structures with periodic aspects (tread lugs), hence an axisymmetric model of everything except the tread shown in the FIG. 19-1a is used in the first step, and then the symmetric model generation option is used to sweep the axisymmetric model about a given axis to create a three-dimensional sector. Next, a 3D mesh of a single tread patch is directly included in the input file with a tie constraint to attach the tread to the revolved sector (FIG. 19-2). In the next step, the feature periodic symmetric model generation is used to create a full 3D model. Also, an Abaqus input file is generated at this step. This input file

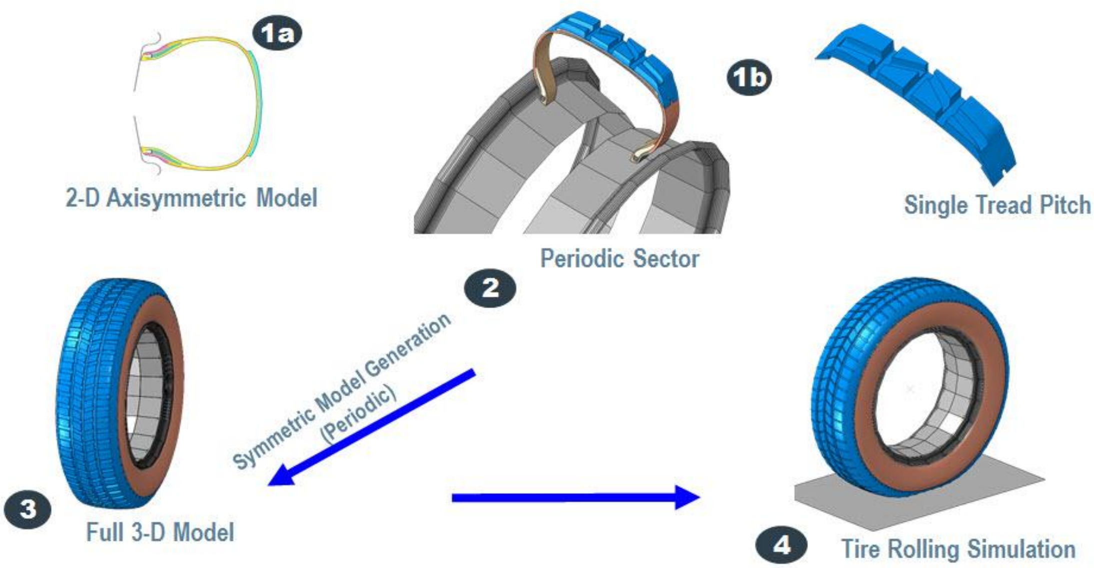


FIG. 19: 3D Tire Model Generation Steps

is then appended with step definitions to carry out tire rolling analysis as discussed in the next section.

## *5.2 Tire Rolling Analysis Approach*

Tire rolling simulation is carried out in a multi-step analysis. In the first step, rim mounting analysis is carried out by applying a small pressure on the bead surface to push the tire inside the rim. In the second step, tire is inflated by applying the desired inflation pressure on the inside surface of the tire. In the third step, the gravity load is applied to the entire model. These analyses are carried out quasi-statically to avoid dynamic effects. In the final step, a prescribed velocity boundary condition is applied to the road.

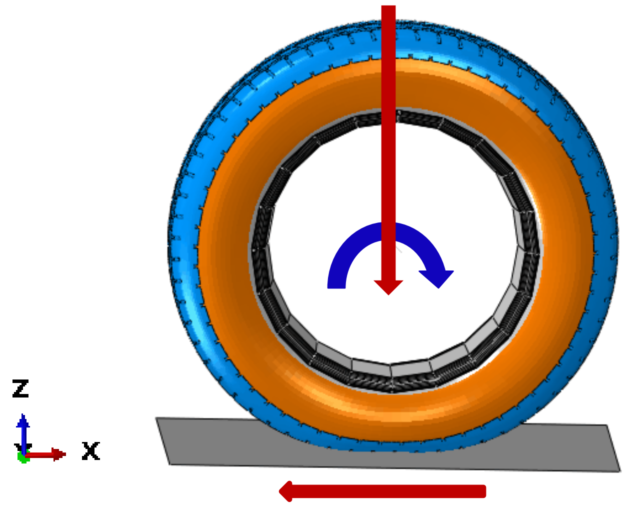


FIG. 20: Tire Rolling Analysis Approach

As the road moves along negative X direction as shown in the FIG. 20, the tire starts rolling clockwise due to the contact between the road and the tire. In this example, tire achieves the full speed of 70 mph by 1 sec.

Normally, an explicit dynamics solution for steady tire rolling is noisy in compared to the steady state transport technique. To reduce the noise in the solution, an axial connector was created at the wheel hub in the vertical direction, and connector behavior with only connector damping is used for this connector. The connector damping coefficient is computed based on the critical damping of a system using the relation $C=2\sqrt{km}$ where C is the damping coefficient, k is stiffness of the tire and m is mass of the tire.

## *5.3 Tire Analysis Results*

A representative passenger tire model was selected to investigate the effect of the nonlinear viscoelasticity of the rubber material. The model was built as described in the previous section. FIG. 21 shows the simulation results of this tire model. The left hand side of FIG. 21 shows the contact pressure when the tire reaches a steady rolling speed of 70 mph. The contact pressure at the footprint looks very smooth and the results demonstrate that a smooth solution is achievable with Explicit Dynamics approach. The right hand side of the FIG. 21 shows creep dissipation energy (ALLCD). Note that Abaqus/Explicit does not compute creep dissipation energy with linear viscoelasticity, and that is why ALLCD is zero with linear viscoelasticity. However, ALLCD is computed correctly with the PRF model. As the tire keeps rolling, energy dissipation due to hysteresis increases steadily.

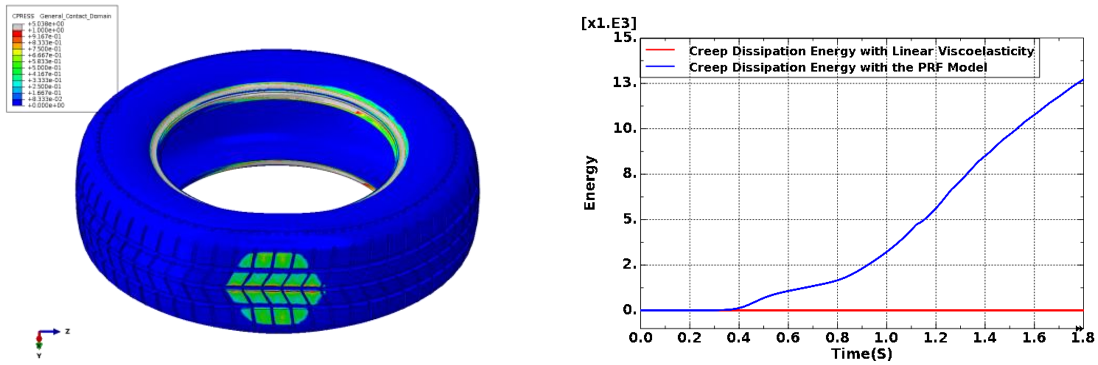


FIG. 21: Contact Pressure and Energy Dissipation Plots

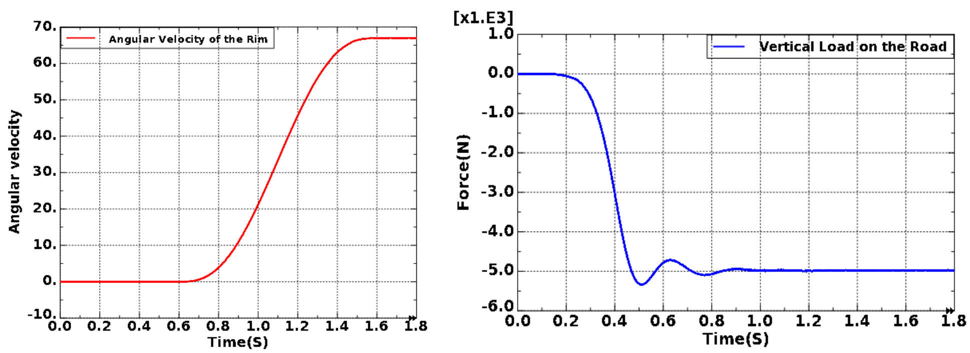


FIG. 22: Angular Velocity and Vertical Load Plots

FIG. 22 shows the angular velocity of the rim and the vertical load on the road. These plots indicate that the noise in the solution has been reduced significantly with the help of connector damping.

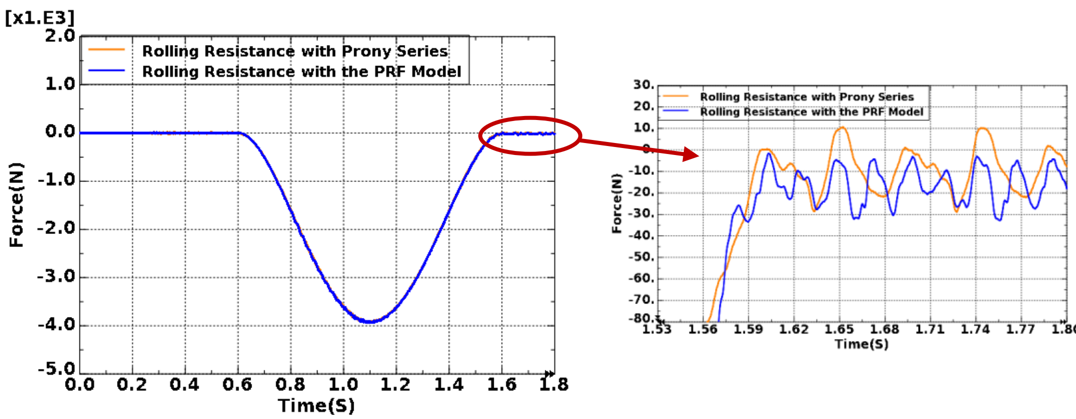


FIG. 23: Rolling Resistance

FIG. 23 shows the rolling resistance with Prony terms and with the  PRF model. Rolling resistance is the force in forward direction (X) when the tire achieves full speed at 1.6 sec. Rolling resistance is predicted to be slightly higher with the PRF model than with the Prony terms for this particular tire model.

### *5.3  Heat Generation and Temperature Prediction*

Due to repeated cyclic loading and viscoelastic energy dissipation, temperature rise can occur at high rolling speed. As the viscoelastic energy dissipation is computed accurately with the PRF model, heat generation and hence the temperature distribution can be computed accurately in tires.

A simple tire model, shown in the FIG. 24, was selected to demonstrate this analysis approach. The tire is modeled with C3D8RT elements. The material definition includes the input for the PRF strain hardening creep law model with conductivity, specific heat and inelastic heat fraction. Assuming that 98 % of the dissipated energy will convert into

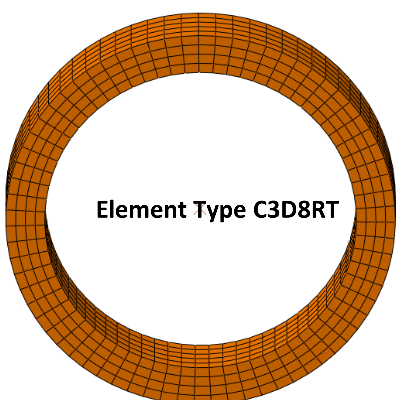


```
*dynamic temperature-displacement, explicit
, 3.0
```

```
*MATERIAL, NAME=MATERIAL-1
*DENSITY
1.1E-09,
*HYPERELASTIC, YEOH, MODULI=INSTANT
1.72270010,-0.908792263,0.532546333, 0.01169, 0., 0
*VISCOELASTIC, NONLINEAR, NETWORKID=1, SRATIO=0.184,
LAW=STRAIN
6.612, 2.662, -.093
*VISCOELASTIC, NONLINEAR, NETWORKID=2, SRATIO=0.225,
LAW=STRAIN
26.493, 3.646, -.147
-----------------------------
*CONDUCTIVITY
.15E-3,
*SPECIFIC HEAT
2.01E+8,
*INELASTIC HEAT FRACTION
.98
```

FIG. 24: Model Setup for Heat Generation and Temperature Prediction

heat, .98 was specified as the inelastic heat fraction. Rolling simulation was carried out as described in the previous section. The viscous energy dissipation per unit volume (CENER) and the temperature distribution in the tire are shown in the FIG. 25.

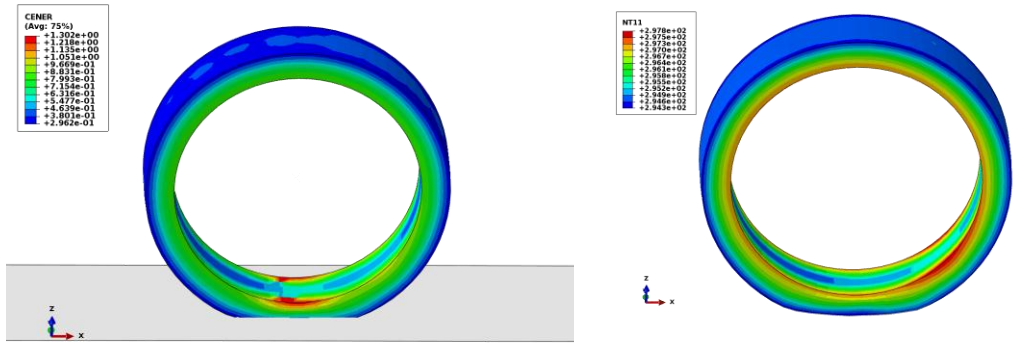


FIG. 25: CENER and Temperature plot

Note that the temperature increase in this analysis is not significant as the tire rolling simulation was carried out for only 3 sec. Also, no heat transfer between the tire and the outside atmosphere was considered in this analysis.

## 6.0 Conclusion

Linear and nonlinear viscoelasticity models available in Abaqus are discussed in the context of tire rolling simulations. An overview of the PRF model with all the available creep laws is also provided. A step-by-step procedure using Isight to calibrate the PRF model parameters starting with stress relaxation test data is provided to help the analysts. The starting point of this calibration procedure is to construct a Hyperelastic and linear viscoelastic model. In the next step, Prony series coefficients are converted into linearized version of the PRF model. The linearized PRF model parameters are a good starting point for the Isight optimization process.

A tire rolling simulation approach using Abaqus/Explicit is presented to take advantage of the PRF model, and a methodology for computing heat generation and predicting temperatures in tires is also briefly discussed.

## 7.0 Future Work

This work can be extended to include heat generation due to the frictional energy dissipation between the tire and the road. Thermal stresses in the tire can also be computed due to heat generation and temperature rise. Furthermore, the authors hope to validate the simulations results with experimental data in future.

## 8.0 Acknowledgements

The authors would like to thank John Lewis from Bridgestone Americas and Juan Hurtado, Harish Surendranath, Murlai Pandheeradi, Fred Arnold, Jegan Chinnaraju and Yangwook Choi from Dassault Systemes SIMULIA Corp. for their encouragements and contributions in writing this paper.

## 9.0 References.


1. Parallel Rheological Framework to model elastomers and Polymers, I. Lapczyk, J.A. Hurtado, and S.M. Govindarajan. Dassault Systèmes Simulia Corp., Providence, RI 02909, U.S.A.
2. Parallel Rheological Framework to model non-linear viscoelasticity, permanent set, and Mullins effect in elastomers J.A. Hurtado & I. Lapczyk *DS SIMULIA Corp.*, S.M. Govindarajan *Veryst Engineering LLC, 47A Kearney Rd, Needham MA 02494 USA*
3. J.S. Bergström, M.C. Boyce, Constitutive modeling of the large strain time-dependent behavior of elastomers, Journal of the Mechanics and Physics of Solids, Vol. 46, Issue 5, 1998, pp. 931-954.
4. J.S. Bergström, M.C. Boyce, Large strain time-dependent behavior of filled elastomers, Mechanics of Materials, Vol. 32, Issue 11, 2000, pp. 627-644.
5. A.S. Khan, O. Lopez-Pamies, R. Kazmi, Thermo-mechanical large deformation response and constitutive modeling of viscoelastic polymers over a wide range of strain rates and temperatures, International Journal of Plasticity, Vol. 22, Issue 4, 2006, pp. 581-601.
6. A.D. Drozdov, A model for the nonlinear viscoelastic response in polymers at finite strains, International Journal of Solids and Structures, Vol. 35, Issue 18, 1998, pp. 2315-2347.
7. P. Haupt A. Lion, E. Backhaus, On the dynamic behaviour of polymers under finite strains: constitutive modelling and identification of parameters, International Journal of Solids and Structures, 37, Issue 26, 2000, pp. 3633-3646.
8. G. A. Holzapfel, J.C. Simo, A new viscoelastic constitutive model for continuous media at finite thermo mechanical changes, International Journal of Solids and Structures, Vol. 33, Issues 20–22, 1996, pp. 3019-3034.
9. Abaqus 6.13. Theory Manual, Dassault Systèmes SIMULIA Corp., Providence, RI, USA, 2013.
10. Abaqus 6.13. User’s Manual, Dassault Systèmes SIMULIA Corp. Providence, RI, USA, 2013.
11. Isight 5.8 User’s Guide, Dassault Systèmes SIMULIA Corp. Providence, RI, USA, 2013.